Calcium oscillations-coupled conversion of actin travelling waves to standing oscillations

Min Wu[1,2], Xudong Wu, and Pietro De Camilli[2]

Howard Hughes Medical Institute, Department of Cell Biology and Program in Cellular Neuroscience, Neurodegeneration and Repair, Yale University School of Medicine, New Haven, CT 06520

Contributed by Pietro De Camilli, December 11, 2012 (sent for review November 9, 2012)

Dynamic spatial patterns of signaling factors or macromolecular assemblies in the form of oscillations or traveling waves have emerged as important themes in cell physiology. Feedback mechanisms underlying these processes and their modulation by signaling events and reciprocal cross-talks remain poorly understood. Here we show that antigen stimulation of mast cells triggers cyclic changes in the concentration of actin regulatory proteins and actin in the cell cortex that can be manifested in either spatial pattern. Recruitment of FBP17 and active Cdc42 at the plasma membrane, leading to actin polymerization, are involved in both events, whereas calcium oscillations, which correlate with global fluctuations of plasma membrane PI(4,5)P_2, are tightly linked to standing oscillations and counteract wave propagation. These findings demonstrate the occurrence of a calcium-independent oscillator that controls the collective dynamics of factors linking the actin cytoskeleton to the plasma membrane. Coupling between this oscillator and the one underlying global plasma membrane PI(4,5)P2 and calcium oscillations spatially regulates actin dynamics, revealing an unexpected pattern-rendering mechanism underlying plastic changes occurring in the cortical region of the cell.

curvature | pattern formation | plasticity | GTPase | frequency

Actin waves have emerged as important cell oscillators that may impact cell polarity (1, 2), motility (3–6), and division (7). Another prominent example of rhythmic cell activity is the oscillations of cytosolic calcium, a second messenger that has also been implicated in these actin-dependent processes, although its precise involvement remains debated (8–11). Calcium oscillations are most strikingly observed in excitatory or secretory cells, but can occur in all cells in response to hormones or growth factors stimulation (12). Though such oscillations provide an attractive mechanism to encode information with frequency and amplitude (13, 14), calcium oscillation-specific functions remain elusive, partially because of the difficulty in dissecting the effects of calcium oscillations from those due to sustained calcium elevations. Considering that rhythmic changes of actin and calcium are likely to have overlapping function in the regulation of fundamental cellular events, here we have investigated their potential coupling in mast cells, a model system where stimulus-evoked changes in cytosolic calcium and actin dynamics have been extensively documented (15). We report the occurrence of both actin waves and actin oscillations in an activity-dependent manner, and the coupling of actin oscillations but not of waves with calcium oscillations. Our results suggest that calcium oscillations, rather than elevation of calcium levels per se, are key factors responsible for the conversion of actin waves into actin oscillations. Thus, calcium oscillations, coupled to PI(4,5)P_2 oscillations, can be used specifically to regulate actin dynamics.

Results and Discussion

Oscillations and Waves of FBP17, Actin, and Cdc42. We first characterized the dynamic actin rearrangements elicited by multivalent antigen cross-linking of Fc receptors on the mast cell surface. Cortical actin in mast cells is represented by a thick and dense network of actin bundles (16). To capture events proximal to assembly sites at the plasma membrane, we imaged FBP17, a potent membrane-associated activator of N-WASP and Arp2/3-dependent actin polymerization (17–19), by total internal reflection fluorescence microscopy (TIRFM). Antigen stimulation produced a striking appearance of FBP17 hotspots in the evanescent field either as recurring waves of hotspots (Fig. 1 *A* and *B*; Movie S1) or as oscillations (Fig. 1 *C* and *D*; Movie S2). The propagation of the waves was due to the sequential formation of new spots at the front of the cluster and disappearance at the back (Fig. 1*B*), with the center of mass of the cluster moving at an average speed of 0.87 μm/s ($n = 70$) and a maximum speed of 1.8 μm/s. During oscillations, hotspots also formed and disassembled sequentially, but the centers of mass of the hotspot ensemble were relatively stationary (Fig. 1*D*). Strictly speaking, oscillations were in fact oscillatory standing waves, although to avoid confusion between the two events, we refer to them as standing oscillations. The periodicity of the two patterns were comparable, with cycles of 29.4 ± 5 s ($n = 12$) or 31.4 ± 4.4 s ($n = 16$) for standing oscillations and traveling waves, respectively.

Oscillations and waves were also observed for actin, as reported both by LifeAct-EGFP (Fig. 2 *A* and *C*; Movie S3) and EGFP-N-WASP (Fig. 2*B*). These cyclic changes did not require the overexpression of FBP17 but were dependent of the polymerization of actin. Addition of latrunculin, which blocks actin polymerization, to cells with traveling waves completely abolished wave propagation (Fig. 2*D*; Movie S3). Antigen stimulation in the presence of latrunculin also failed to trigger oscillations or waves (Fig. S1*A*). Thus, although the peak of actin was delayed by ~3–6 s compared with that of FBP17 (Fig. 2*C*), an actin-dependent positive feedback mechanism was required for pattern initiation and propagation.

Biochemical studies have demonstrated the activation of the small GTPase Cdc42 in mast cells in response to antigen stimulation (20). Cdc42 is a key regulator of actin dynamics, whose reported effectors in mediating such regulation include N-WASP and the FBP17 homologs Toca1 (21) and CIP4 (22). We have now demonstrated that FBP17 as well is a Cdc42 effector, because purified FBP17 binds to the active form of Cdc42, i.e., to GTPγS-bound Cdc42 or to a constitutively active Cdc42 mutant (Fig. 2*E*). Thus, we examined whether the activation of Cdc42 in response to stimulation occurred in pulses. TIRFM analysis of a fluorescent activity sensor of Cdc42 (23) revealed that antigen stimulation of mast cells induced the rapid translocation of this

Author contributions: M.W. designed research; M.W. and X.W. performed research; M.W. contributed new reagents/analytic tools; M.W. analyzed data; and M.W. and P.D.C. wrote the paper.

The authors declare no conflict of interest.

Freely available online through the PNAS open access option.

[1]Present address: Department of Biological Sciences, Centre for BioImaging Sciences, and Mechanobiology Institute, National University of Singapore, Republic of Singapore 117546.

[2]To whom correspondence may be addressed. E-mail: dbswum@nus.edu.sg or pietro.decamilli@yale.edu.

This article contains supporting information online at www.pnas.org/lookup/suppl/doi:10.1073/pnas.1221538110/-/DCSupplemental.

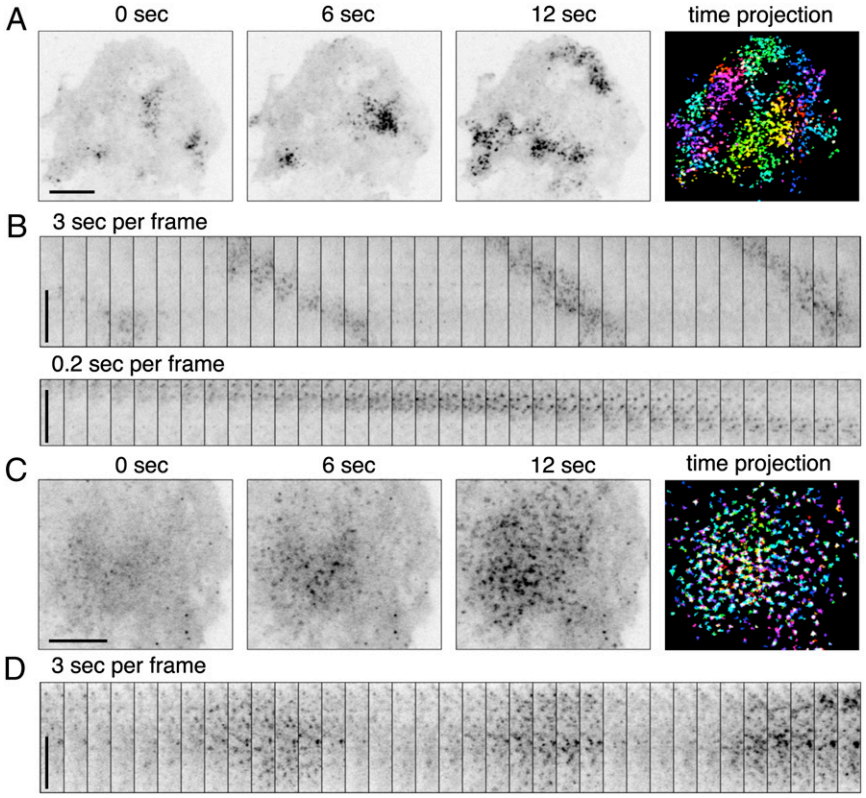

Fig. 1. Traveling waves or standing oscillations of FBP17 in antigen-stimulated mast cells visualized by TIRFM. (*A* and *B*) Waves. (*A*) Three individual frames from a movie of mCherry-FBP17 waves (Movie S1). An inverted grayscale lookup table was used, and fluorescence is shown in black. (*Far Right*) Color image showing superimposition of fluorescence signal from 10 different frames (3-s intervals) of the cell on the *Far Left*, where bright puncta in the same frame are shown in the same color. (*B*) Montage of 35 frames (3 s or 0.2-s intervals) of a small region of the cell showing that wave propagation is through sequential formation and disassembly of puncta. (*C* and *D*) Oscillations. (*C*) Three individual frames from a movie of a mCherry-FBP17 oscillation. (*Far Right*) Color image showing superimposition of fluorescence signal from 10 different frames (3-s intervals) of the cell shown on the *Far Left*, with color-coding based on time as in *A*. (*D*) Montage of 35 frames (3-s intervals) of a small region of the cell showing the cyclic assembly of mCherry-FBP17 puncta at the cell cortex. (Scale bar: 10 μm.)

sensor to the plasma membrane, followed by either oscillations or waves (Fig. 2*F*). Importantly, waves of active Cdc42 overlapped with FBP17 waves both temporally and spatially (Fig. 2*G*; Movie S4), although the appearance of the fluorescence within the waves was diffuse for Cdc42 and punctate for FBP17. These findings strongly support a role of transient local activation of Cdc42 in facilitating the recruitment and polymerization of FBP17 at the plasma membrane.

Oscillations but Not Waves Are Coupled to Calcium Oscillations. Standing oscillations of FBP17 were strictly stimulation-dependent. They started as early as minutes after the beginning of the stimulus (Fig. 3*A*) and were observed up to an hour. In contrast, FBP17 waves occasionally occurred spontaneously without stimuli, although these spontaneous waves had slightly longer periods (40.6 ± 10.5 s, $n = 9$) than stimulus-evoked waves (31.4 ± 4.4 s, $n = 16$; $P < 0.005$, Student t test. These differences led us to speculate that standing oscillations may require additional factors relative to traveling waves.

Antigen stimulation of RBL-2H3 cells frequently induces cytosolic calcium oscillations (24, 25), whose time of onset relative to the stimulus, and duration, are heterogeneous (Fig. S2). In all cells where FBP17 oscillations occurred ($n = 12$), oscillatory calcium spikes were also detected, as shown by the calcium sensor GCaMP3 (26) (Fig. 3*A*; Movie S5). Fourier transforms of both oscillations revealed a precisely matching frequency component (Fig. 3*A*), whereas the phases were roughly anticorrelated (Fig. 3*C*). However, the elevation of cytosolic calcium alone was not sufficient to induce FBP17 recruitment, and regulated calcium dynamics was required for oscillations of FBP17. Presence of thapsigargin (which depleted intracellular calcium stores) during antigen stimulation completely abolished both calcium oscillations and FBP17 oscillations (Fig. S1*B*). Calcium oscillations often started after a broad and prolonged calcium peak due to depletion of intracellular stores (Fig. 3*A*), but this initial calcium elevation did not induce FBP17 recruitment; rather, in many cases, this corresponded to a decrease in the FBP17 intensity (Figs. 3*A* and 4). In addition, the rise and fall of the FBP17 signal during each oscillation occurred when calcium level remained in the baseline (Fig. 3*C*). These findings suggested that calcium itself was unlikely to be the rate-limiting step in the regulation of the FBP17 oscillations, and that factors linking both calcium and FBP17 may be responsible for their identical frequency.

Calcium oscillations can be coupled with oscillations of IP_3 via a feedback loop that involves the calcium-dependent hydrolysis of $PI(4,5)P_2$ by phospholipase C (12). $PI(4,5)P_2$, which is concentrated in the plasma membrane, plays a major role in the recruitment and activation at this membrane of actin regulatory proteins and thus in actin nucleation (27); it is also thought to have a direct role in the membrane recruitment of FBP17 (17, 18). To determine whether $PI(4,5)P_2$ links calcium spikes to FBP17 oscillations, levels of this phosphoinositide in the plasma membrane were monitored by TIRFM using mRFP-$PH_{PLC\delta}$, a $PI(4,5)P_2$ reporter. $PI(4,5)P_2$ started to oscillate after an antigen stimulation-dependent initial $PI(4,5)P_2$ drop. This initial drop was shown to be due to the activation of phospholipase C (28), which is consistent with an absence of FBP17 recruitment in this initial phase of stimulation. $PI(4,5)P_2$ oscillations were cell-wide (Fig. 3*B*) and anticorrelated with calcium oscillation,

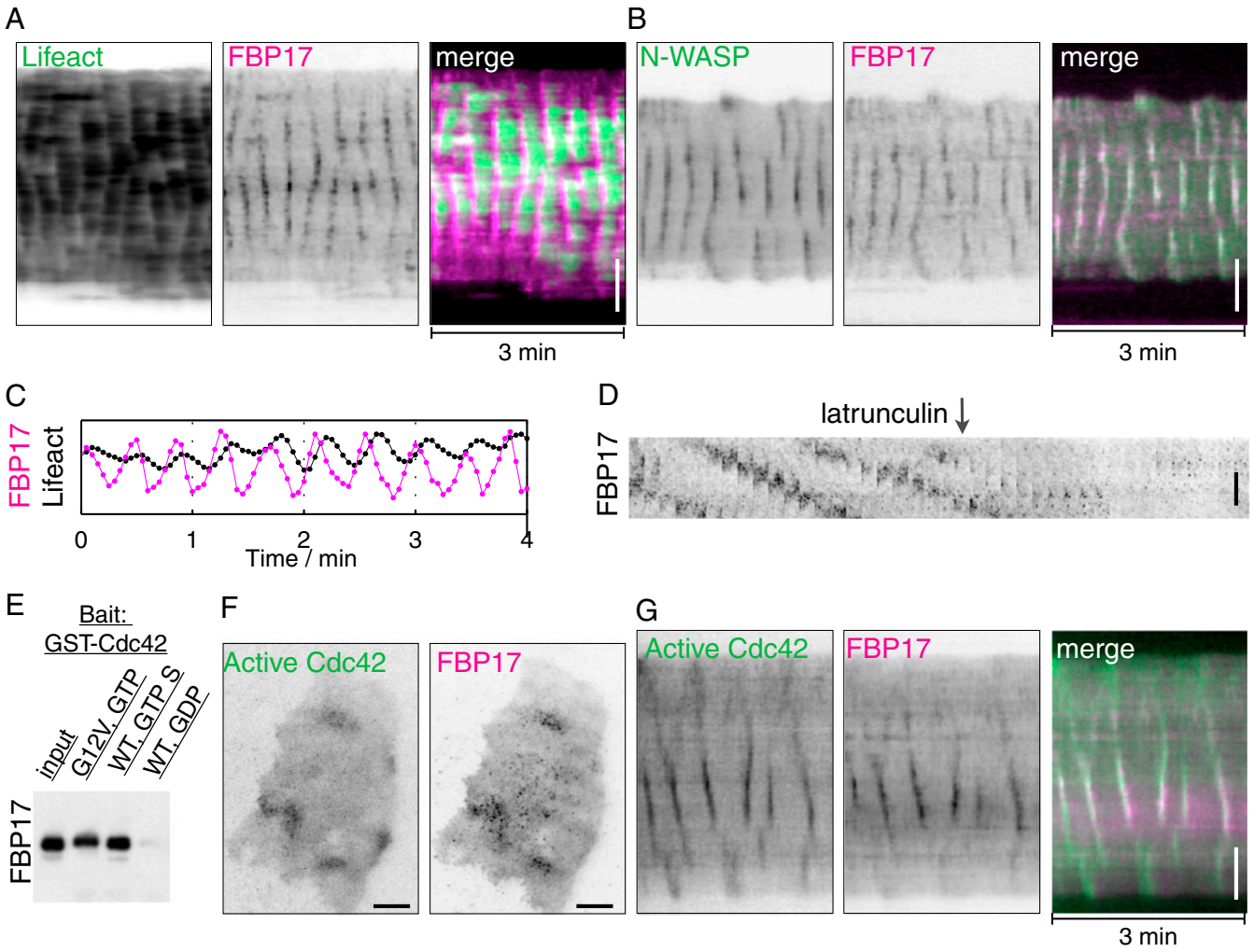

Fig. 2. Stimulus-evoked waves of FBP17 are synchronized with both N-WASP and active Cdc42 and require actin polymerization. (*A* and *B*) Kymographs of actin (LifeAct-GFP), N-WASP-GFP, and mCherry-FBP17 waves. (*C*) Relative phase-shifts of FBP17 and actin. Peaks of FBP17 preceded actin by 3–6 s. (*D*) Montage of sequential frames from a portion of a cell expressing mCherry-FBP17 showing that addition of latrunculin abolished waves (Movie S3). (*E*) FBP17 is a Cdc42 effector in vitro. Binding assay showing that purified FBP17 interacts with the purified active form of Cdc42, i.e., with GTPγS-bound Cdc42 or with a constitutively active GTP-bound Cdc42 mutant, but not to GDP-bound Cdc42. (*F*) Snapshots of a cell with antigen-evoked traveling waves show that the diffuse but locally concentrated accumulation of active Cdc42 at the plasma membrane (Cdc42 CBD-EGFP) coincides with clusters of FBP17 puncta. (*G*) Kymograph from a movie of traveling waves showing coupled dynamics of FBP17 and active Cdc42 (Movie S4). An inverted lookup table was used for grayscale images and kymographs. (Scale bar: 10 μm.)

similar to FBP17 oscillations (Fig. 3*C*). Thus, $PI(4,5)P_2$ may represent a key upstream factor that coordinates calcium and FBP17/actin oscillations.

Though calcium oscillations with matching frequencies were observed in all cells with FBP17 oscillations ($n = 12$), demonstrating a tight coupling between the two processes, they only occurred in 21% of the cells with FBP17 waves (5 of 24 cells). Of the other cells in this group ($n = 19$), 53% had no detectable calcium fluctuations ($n = 10$; e.g., Fig. S3 *A* and *B* before stimulation) and 47% had intermittent and weak calcium pulses whose frequencies did not match those of the FBP17 waves ($n = 9$; e.g., Fig. S3*B* after stimulation). This lack of strong coupling between calcium oscillations and traveling waves of FBP17 adds further evidence for the lack of a direct cause–effect relationship between levels of cytosolic calcium and FBP17 recruitment to the cell cortex.

Consistent with the dissociation between traveling waves and calcium oscillations, there were no global $PI(4,5)P_2$ oscillations or local $PI(4,5)P_2$ waves (as detected by the $PI(4,5)P_2$ reporter mRFP-$PH_{PLC\delta}$) in cells with traveling waves. Dynamic turnover of $PI(4,5)P_2$, resulting in changes too shallow to be revealed by mRFP-$PH_{PLC\delta}$, may occur at waves, likely coordinated by cycles of phosphorylation/dephosphorylation by PI4P 5-kinases and $PI(4,5)P_2$ phosphatases, respectively. Importantly, however, the feedback loop involving FBP17, Cdc42, and actin can apparently act independently from that controlling cell-wide calcium oscillations, which involves the activation of phospholipase C and results in detectable $PI(4,5)P_2$ oscillations (Fig. 5).

Interconversion Between Oscillations and Waves. To determine whether these different actin dynamic spatial patterns (oscillations and waves) reflect heterogeneity of the cell population or differential activity states of the cell, we examined if they can interconvert within the same cell. Cells that displayed spontaneous FBP17 waves with little or no calcium pulses were stimulated with antigen, to elicit calcium/$PI(4,5)P_2$ oscillations. In cells that generated robust calcium oscillations (Fig. 4*A*), FBP17 waves became synchronized into a cell-wide standing oscillatory pattern after a brief pause (Fig. 4*B*; Movie S6). Conversely, in cells where traveling waves resumed after such pause, calcium oscillations

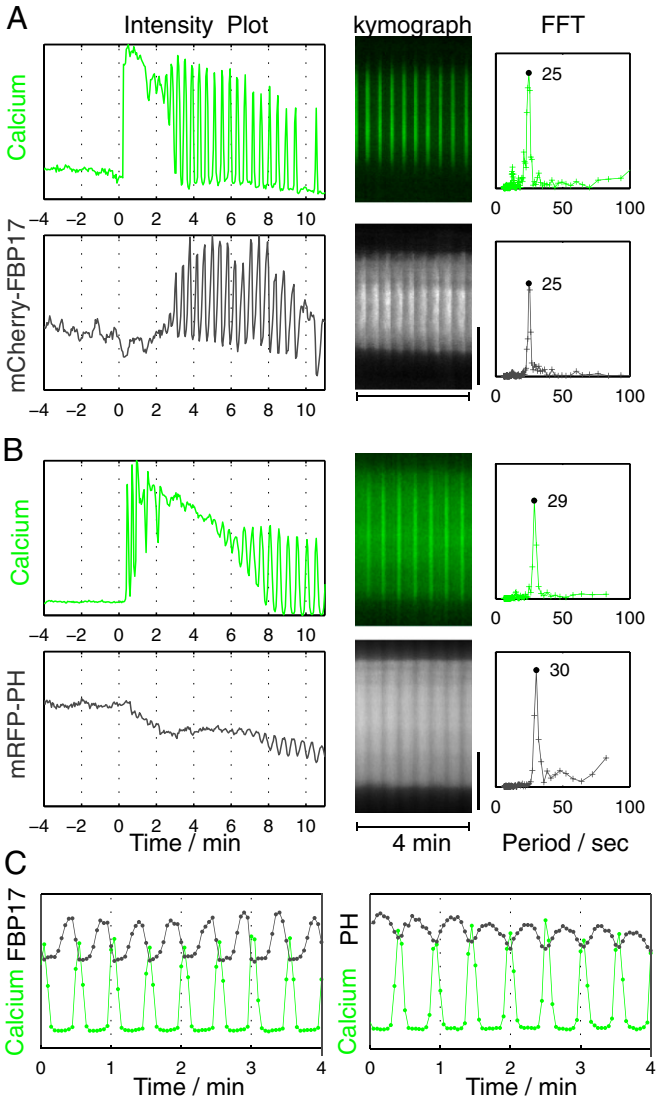

Fig. 3. Stimulation-dependent oscillations of FBP17 and PI(4,5)P_2 and their relation to calcium oscillations. (*A*) (*Left*) Antigen stimulation produced an increase in the recruitment of mCherry-FBP17, which occurred as standing oscillations. Oscillations started after a sustained increase in cytosolic calcium (as detected by the calcium sensor GCaMP3), when calcium itself started to oscillate. (*Center*) Kymograph showing that oscillations not only of calcium but also of FBP17 occur synchronously throughout the cell. (*Right*) Power spectrum, based on the Fourier transforms (FFT), of calcium and mCherry-FBP17 oscillations indicating a single matching frequency. (*B*) Stimulation triggered oscillations of plasma membrane PI(4,5)P_2, as imaged by mRFP-$PH_{PLC\delta}$. *Center* and *Right* are as in *A*. (*C*) Both FBP17 and PI(4,5)P_2 were opposite in phase relative to calcium. In *A* and *B*, time 0 is the time of antigen addition. (Scale bar: 10 μm.)

were either not engaged or uncorrelated (see poststimulation periods in Fig. S3 *A* and *B*, respectively), indicating the coupling with calcium oscillations may be necessary for the conversion. A switch of the FBP17 fluorescence signal from traveling waves to standing oscillations and vice versa could also occur spontaneously during the poststimulation period (Fig. S3*C*; Movie S7). When this occurred, bursts of standing FBP17 oscillations correlated with bursts of calcium oscillations, which were instead absent during periods of FBP17 waves. Thus, robust oscillations of calcium that correlate with PI(4,5)P_2 oscillations appear to convert a traveling wave into a cell-wide standing oscillation.

How can the presence of global calcium/PI(4,5)P_2 oscillations change the dynamic spatial pattern of actin? During standing oscillations, i.e., when cell-wide PI(4,5)P_2 oscillations are observed, cyclic changes of FBP17 fluorescence intensities in the evanescent field (Fig. 4*C*) were contributed both by oscillation of the punctate signal (Fig. 4*D*), reflecting cycles of assembly and disassembly of FBP17 hot spots, and by oscillations of the diffuse signal (Fig. 4*E*), reflecting global FBP17 binding to the membrane that correlates with PI(4,5)P_2 levels. In contrast, only the punctate signal, but not the global diffuse signal, underwent fluctuations during waves, when the PI(4,5)P_2 signal detectable by mRFP-$PH_{PLC\delta}$ does not oscillate. The wave to oscillation transition precisely matched the onset of cell-wide oscillations of the diffuse plasma membrane-associated FBP17 fluorescence (Fig. 4). Though both standing oscillations and traveling waves involve coordinated bindings and dissociations of FBP17, Cdc42, and actin at the membrane, the directionality of wave propagation may require significant asynchrony between factors that control assembly (at the front of the wave) and factors that control dissociation (at the back of the wave) (29). Such spatially restricted dynamic changes will be overridden by a cell-wide diffuse signal that acts upstream. The robust oscillations of PI(4,5)P_2 that occur

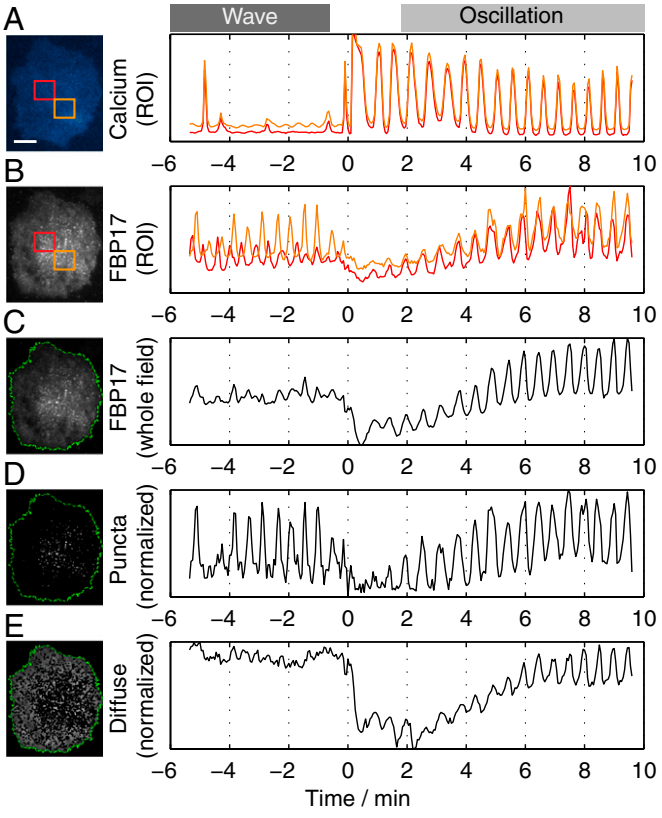

Fig. 4. Conversion of spontaneous traveling waves to global standing oscillations in response to a stimulus are coupled with the onset of calcium oscillations. (*A*) Robust calcium oscillations elicited by antigen stimulation. (*B*) Analysis of local FBP17 fluorescence in ROIs (orange and red squares in the micrograph) demonstrates that fluctuations in the two ROIs are not in phase before the stimulus (waves), but become synchronized after stimulation (oscillations; Movie S6). (*C*) Fluctuations of total FBP17 fluorescence intensities in the whole TIRFM field are more pronounced after stimulation. (*D*) Fluctuations of the punctate signal (white dots), normalized using the total punctate area, display a similar amplitude during waves and oscillations. (*E*) Oscillation of the diffuse FBP17 fluorescence (the fluorescence surrounding the puncta), normalized using the total diffuse pool area, only occurred during calcium oscillations and correlated with the conversion of traveling waves into standing oscillations. Time 0 is the time of antigen addition. (Scale bar: 10 μm.)

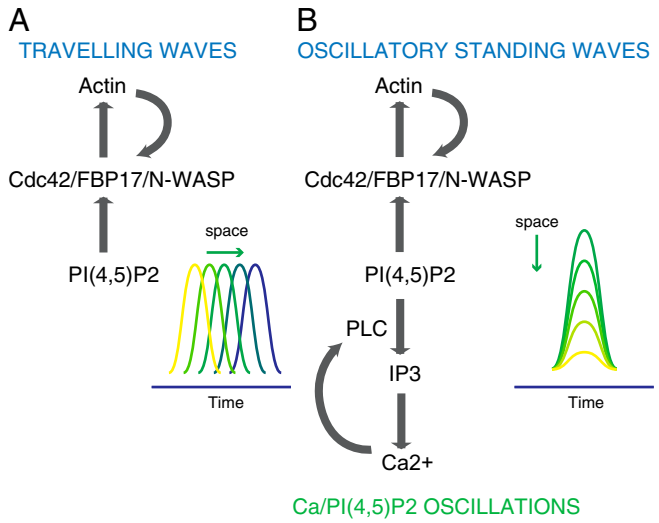

Fig. 5. Schematic representation of the mechanisms underlying the traveling waves and standing oscillations. (*A*) Traveling waves involve actin-dependent positive-feedback mechanisms that are calcium independent. (*B*) Actin oscillations require similar molecular components as actin waves, but are coupled with calcium oscillations, likely via $PI(4,5)P_2$ oscillations.

during calcium oscillations likely represent the signal that modulates globally the dynamics of proteins associated with the plasma membrane.

Concluding Remarks. Feedback regulatory loops underlying oscillations or waves have been increasingly recognized as important factors in the organization of signaling events (30). The oscillatory nature of the recruitment and assembly of actin regulatory proteins and actin, via the control of reversible and low-affinity interactions, may facilitate the occurrence of adaptive modifications in the actin cortex and the plasma membrane. This plasticity may be particularly important following stimulation—an event that involves dramatic cell shape changes, actin reorganization, regulated secretion, and compensatory endocytosis (15). In this context, it is important to note that calcium oscillations induced by stimulation in mast cells and other secretory cells were shown to correlate with oscillatory bursts of secretion (31–33). Interestingly, FBP17 is an F-BAR domain-containing protein (34) that can participate in endocytosis (35, 36). Though feedback regulatory mechanisms mediated by Cdc42 activation and actin polymerization are involved in the collective events described here, irrespective of their spatial pattern, they can be coupled to, or decoupled from, those underlying calcium oscillations, resulting in either standing oscillations or traveling waves (Fig. 5). The integration of distinct oscillatory systems may be of general importance in fine-tuning cell plasticity by spatially controlling membrane and cytoskeleton dynamics.

Methods

Materials. RBL-2H3 cells (tumor mast cells), mouse monoclonal anti–2,4-dinitrophenyl (DNP) IgE, and the multivalent antigen DNP-BSA were generous gifts from Barbara Baird and David Holowka (Cornell University, Ithaca, NY). The following reagents were obtained from commercial sources: GTP and GDP from Sigma; GTPgS from Roche; and thapsigargin and latrunculin B from Calbiochem. Polyclonal anti-FBP17 antibodies were previously described (17). Constructs for the following proteins were kind gifts: mCherry-FBP17 from Pontus Aspenstrom (Karolinska Institutet, Stockholm); mRFP-$PH_{PLC\delta}$ (pleckstrin homology domain of PLC_δ) from Sergio Grinstein (University of Toronto, Toronto); LifeAct-EGFP from Roland Wedlich-Soldner (Max Planck Institute of Biochemistry, Martinsried, Germany); GST-Cdc42 G12V and GST-Cdc42 WT from Tony Koleske (Yale University, New Haven, CT); CBD-GFP, a Cdc42 activity probe (generated by cloning bacterial expressing Cdc42 activity sensor pET23-CBD-(-PP)-EGFP (23) (Addgene no. 12597) into pEGFP-N1 vector with restriction sites XhoI and BamH1) from Hongying Shen (our laboratory). GCAMP3 (26) was from Addgene (no. 22692). FBP17-EGFP was prepared by cloning EGFP-FBP17 (17) into the pEGFP-N1 vector using the BamH1 and HindIII restriction sites. GST-FBP17 (17) was previously described.

Cell Culture and Transfection. RBL-2H3 cells were maintained in monolayer cultures and harvested with trypsin-EDTA (Life Technologies) 3–5 d after passage. Transient transfections were carried out on cells in suspension using program X-01 of the Amaxa electroporator (Lonza). After transfection, cells were plated at subconfluent densities in 35-mm Petri dishes with coverglass bottoms (MatTek) and sensitized with anti-DNP IgE at 0.4 μg/mL overnight. Typically cells were cultured for 12–24 h and washed twice in buffered saline solution [135 mM NaCl, 5.0 mM KCl, 1.8 mM $CaCl_2$, 1.0 mM $MgCl_2$, 5.6 mM glucose, 20 mM Hepes (pH 7.4)] containing 1 mg/mL BSA before imaging; they were subsequently transferred to a homemade heated microscope stage maintained at 37 °C through a bipolar temperature controller (Harvard Apparatus). In all experiments, cells were stimulated with 100 ng/mL DNP-BSA. For experiments using inhibitors, latrunculin B and thapsigargin were diluted from the stock solution and added to the adherent cells at a final concentration of 12.5 μM and 2 μM, respectively.

TIRFM. A Nikon Ti-E inverted microscope equipped with Perfect Focus system, motorized illumination unit, and iXon 897 Electron Multiplying Charge Coupled Device (EMCCD) camera (Andor Technologies) was used. All images were acquired through an Olympus TIRFM objective (CFI Apochromat 100×, N.A. 1.49). Samples were excited with 488-nm/50-mW and 561-nm/50-mW diode lasers sequentially, and two-color images were acquired through a dual-bandpass filter (exciter: 468/34, 553/24 nm; emitter: 512/23, 630/91 nm; Semrock). Andor IQ software was used to acquire data at binning 2.

Image Analysis. ImageJ (National Institutes of Health) was used for generating montages, kymographs, and quantification based on manually selected regions of interest (ROIs). MatLab (MathWorks) was used for frequency analysis and quantification requiring image segmentation. For the identification of the frequency components of an intensity profile, the built-in fast Fourier transform function in MatLab was used. For quantification involving image segmentation, including global analysis of a single cell and analysis of puncta intensity vs. diffuse signals, custom-written algorithms was used (37). Briefly, a median filter was applied to each frame of the image series and the field of view was segmented into two regions: "cell" and "background" by thresholding and morphological operations. All pixels positive for cell were subsequently segmented into puncta (identified as pixels with intensity above their local background by a threshold value A) and diffuse (defined as pixels not greater than their local background by a threshold value B) by local background subtraction, peak identification, and thresholding. B is set at a smaller value than A to reduce the contamination of the signals from the puncta into diffuse pool. The defined puncta and cell boundaries were overlaid with the original movie for visual inspection. The number of pixels defined as puncta or diffuse, and their average intensities, were plotted against time.

Statistical Analyses. Statistical analyses were performed with the unpaired two-tailed Student *t* test. Average data are expressed as mean ± SEM.

Protein Biochemistry. GST fusion proteins (Cdc42 wt, Cdc42 G12V, and FBP17) were bacterially expressed and purified using Glutathione Sepharose 4B beads (Amersham Biosciences) according to the manufacturer's instructions. GST-Cdc42 WT and Cdc42 G12V were eluted from the beads and incubated with fresh beads to reach saturation of the bead capacity. For nucleotide loading, these GST-Cdc42–loaded beads were incubated in buffer A (PBS plus 2.5 mM $MgCl_2$) with 2.5 mM GTP, GDP, or GTPγS at 30 °C for 20 min. Beads were then washed twice with buffer A, and the supernatant was removed. For in vitro binding, the GST tag of FBP17 was removed using PreScission protease (Amersham Biosciences), and fresh beads were used to remove free GST and uncleaved GST-FBP17. Cleaved FBP17 (0.5–1 mg/mL, 200 μL) was incubated with GST-Cdc42 beads loaded with nucleotides in buffer A with 0.1% Triton X at 4 °C for 2 h. Then, beads were washed once with buffer A + 0.25% Triton X and twice with buffer A + 0.1% Triton X. Total protein was eluted with SDS/PAGE sample loading buffer. A total of 5% (vol/vol) of the eluted mixture and 0.5% of input were loaded for Western blot analysis.

ACKNOWLEDGMENTS. We thank Hongying Shen, Francesca Giordano, and other members of P.D.C.'s laboratory for discussions, and F. Wilson, S. Wilson, and M. Graham for technical support. This work was supported in part by National Institutes of Health Grants R37NS036251, DK45735, and DK082700.

1. Ozbudak EM, Becskei A, van Oudenaarden A (2005) A system of counteracting feedback loops regulates Cdc42p activity during spontaneous cell polarization. *Dev Cell* 9(4):565–571.
2. Millius A, Dandekar SN, Houk AR, Weiner OD (2009) Neutrophils establish rapid and robust WAVE complex polarity in an actin-dependent fashion. *Curr Biol* 19(3):253–259.
3. Giannone G, et al. (2004) Periodic lamellipodial contractions correlate with rearward actin waves. *Cell* 116(3):431–443.
4. Schroth-Diez B, et al. (2009) Propagating waves separate two states of actin organization in living cells. *HFSP J* 3(6):412–427.
5. Weiner OD, Marganski WA, Wu LF, Altschuler SJ, Kirschner MW (2007) An actin-based wave generator organizes cell motility. *PLoS Biol* 5(9):e221.
6. Case LB, Waterman CM (2011) Adhesive F-actin waves: A novel integrin-mediated adhesion complex coupled to ventral actin polymerization. *PLoS ONE* 6(11):e26631.
7. Mitsushima M, et al. (2010) Revolving movement of a dynamic cluster of actin filaments during mitosis. *J Cell Biol* 191(3):453–462.
8. Wei C, et al. (2009) Calcium flickers steer cell migration. *Nature* 457(7231):901–905.
9. Wedlich-Soldner R, Li R (2003) Spontaneous cell polarization: Undermining determinism. *Nat Cell Biol* 5(4):267–270.
10. Traynor D, Milne JL, Insall RH, Kay RR (2000) Ca(2+) signalling is not required for chemotaxis in Dictyostelium. *EMBO J* 19(17):4846–4854.
11. Evans JH, Falke JJ (2007) Ca2+ influx is an essential component of the positive-feedback loop that maintains leading-edge structure and activity in macrophages. *Proc Natl Acad Sci USA* 104(41):16176–16181.
12. Harootunian AT, Kao JP, Paranjape S, Tsien RY (1991) Generation of calcium oscillations in fibroblasts by positive feedback between calcium and IP3. *Science* 251(4989):75–78.
13. Li W, Llopis J, Whitney M, Zlokarnik G, Tsien RY (1998) Cell-permeant caged InsP3 ester shows that Ca2+ spike frequency can optimize gene expression. *Nature* 392 (6679):936–941.
14. Dolmetsch RE, Xu K, Lewis RS (1998) Calcium oscillations increase the efficiency and specificity of gene expression. *Nature* 392(6679):933–936.
15. Pfeiffer JR, Seagrave JC, Davis BH, Deanin GG, Oliver JM (1985) Membrane and cytoskeletal changes associated with IgE-mediated serotonin release from rat basophilic leukemia cells. *J Cell Biol* 101(6):2145–2155.
16. Andrews NL, et al. (2008) Actin restricts FcepsilonRI diffusion and facilitates antigen-induced receptor immobilization. *Nat Cell Biol* 10(8):955–963.
17. Itoh T, et al. (2005) Dynamin and the actin cytoskeleton cooperatively regulate plasma membrane invagination by BAR and F-BAR proteins. *Dev Cell* 9(6):791–804.
18. Tsujita K, et al. (2006) Coordination between the actin cytoskeleton and membrane deformation by a novel membrane tubulation domain of PCH proteins is involved in endocytosis. *J Cell Biol* 172(2):269–279.
19. Takano K, Toyooka K, Suetsugu S, Suetsugu S (2008) EFC/F-BAR proteins and the N-WASP-WIP complex induce membrane curvature-dependent actin polymerization. *EMBO J* 27(21):2817–2828.
20. El-Sibai M, Backer JM (2007) Phospholipase C gamma negatively regulates Rac/Cdc42 activation in antigen-stimulated mast cells. *Eur J Immunol* 37:261–270.
21. Ho H-YH, et al. (2004) Toca-1 mediates Cdc42-dependent actin nucleation by activating the N-WASP-WIP complex. *Cell* 118(2):203–216.
22. Aspenström P (1997) A Cdc42 target protein with homology to the non-kinase domain of FER has a potential role in regulating the actin cytoskeleton. *Curr Biol* 7(7): 479–487.
23. Nalbant P, Hodgson L, Kraynov V, Toutchkine A, Hahn KM (2004) Activation of endogenous Cdc42 visualized in living cells. *Science* 305(5690):1615–1619.
24. Millard PJ, Ryan TA, Webb WW, Fewtrell C (1989) Immunoglobulin E receptor cross-linking induces oscillations in intracellular free ionized calcium in individual tumor mast cells. *J Biol Chem* 264(33):19730–19739.
25. Cohen R, Torres A, Ma H-T, Holowka D, Baird B (2009) Ca2+ waves initiate antigen-stimulated Ca2+ responses in mast cells. *J Immunol* 183(10):6478–6488.
26. Tian L, et al. (2009) Imaging neural activity in worms, flies and mice with improved GCaMP calcium indicators. *Nat Methods* 6(12):875–881.
27. Di Paolo G, De Camilli P (2006) Phosphoinositides in cell regulation and membrane dynamics. *Nature* 443(7112):651–657.
28. Stauffer TP, Ahn S, Meyer T (1998) Receptor-induced transient reduction in plasma membrane PtdIns(4,5)P2 concentration monitored in living cells. *Curr Biol* 8(6): 343–346.
29. Loose M, Fischer-Friedrich E, Herold C, Kruse K, Schwille P (2011) Min protein patterns emerge from rapid rebinding and membrane interaction of MinE. *Nat Struct Mol Biol* 18(5):577–583.
30. Brandman O, Meyer T (2008) Feedback loops shape cellular signals in space and time. *Science* 322(5900):390–395.
31. Tse A, Tse FW, Almers W, Hille B (1993) Rhythmic exocytosis stimulated by GnRH-induced calcium oscillations in rat gonadotropes. *Science* 260(5104):82–84.
32. Kim TD, Eddlestone GT, Mahmoud SF, Kuchtey J, Fewtrell C (1997) Correlating Ca2+ responses and secretion in individual RBL-2H3 mucosal mast cells. *J Biol Chem* 272(50): 31225–31229.
33. Cohen R, Corwith K, Holowka D, Baird B (2012) Spatiotemporal resolution of mast cell granule exocytosis reveals correlation with Ca2+ wave initiation. *J Cell Sci* 125(Pt 12): 2986–2994.
34. Shimada A, et al. (2007) Curved EFC/F-BAR-domain dimers are joined end to end into a filament for membrane invagination in endocytosis. *Cell* 129(4):761–772.
35. Wu M, et al. (2010) Coupling between clathrin-dependent endocytic budding and F-BAR-dependent tubulation in a cell-free system. *Nat Cell Biol* 12(9):902–908.
36. Giuliani C, et al. (2009) Requirements for F-BAR proteins TOCA-1 and TOCA-2 in actin dynamics and membrane trafficking during Caenorhabditis elegans oocyte growth and embryonic epidermal morphogenesis. *PLoS Genet* 5(10):e1000675.
37. Wu M, Holowka D, Craighead HG, Baird B (2004) Visualization of plasma membrane compartmentalization with patterned lipid bilayers. *Proc Natl Acad Sci USA* 101(38): 13798–13803.